Raman scattering in a Heisenberg $S = \frac{1}{2}$ antiferromagnet on the anisotropic triangular lattice

Natalia B. Perkins,[1] Gia-Wei Chern,[1,2] and Wolfram Brenig[3]

[1]*Department of Physics, University of Wisconsin-Madison, Madison, Wisconsin 53706, USA*

[2]*Theoretical Division, Los Alamos National Laboratory, Los Alamos, New Mexico 87545, USA*

[3]*Institute for Theoretical Physics, Technical University Braunschweig, Mendelssohnstr. 3, 38106 Braunschweig, Germany*

We investigate the two-magnon Raman scattering from an anisotropic $S = \frac{1}{2}$ triangular Heisenberg antiferromagnet Cs_2CuCl_4. We find that the Raman response is very sensitive to magnon-magnon interactions and to scattering geometries, a feature that is in remarkable contrast with the polarization-independent Raman signal from the isotropic triangular Heisenberg antiferromagnet. Since a spin-liquid ground state gives rise to a similar rotationally invariant Raman response, our results on the polarization dependence of the scattering spectrum suggest that Raman spectroscopy provides a useful probe, complementary to neutron scattering, of the ground-state properties of Cs_2CuCl_4, particularly whether the time-reversal symmetry is broken in the ground state.

PACS number(s): 78.30.−j, 75.10.Jm, 75.25.−j

I. INTRODUCTION

Recently, Heisenberg antiferromagnets on the triangular lattice have attracted considerable experimental and theoretical interest. Among them, Cs_2CuCl_4 has been under particular scrutiny as it provides an interesting example of a spatially anisotropic spin-$\frac{1}{2}$ triangular antiferromagnet.[1–10] Much of the interest in this compound stems from its unusual, nonclassical magnetic properties, arising from the competition between the spatial anisotropy, Dzyaloshinskii-Moriya (DM) interactions, and quantum fluctuations.

Extensive neutron scattering studies[1,2] on the magnetic properties of Cs_2CuCl_4 revealed several interesting features. First, despite frustration and low dimensionality, a long-range magnetic order develops at low temperatures: the observed spin order is incommensurate and sets in at temperatures below $T_N = 0.62$ K. Magnetic excitations above this ground state are also quite unusual. While the low-energy excitation spectrum contains well-defined sharp modes, as expected for an ordered state, a broad continuum is formed at intermediate and high energies. A number of theoretical proposals have been made to explain the origin of this continuum. It has been suggested that the existence of a continuum is an indication that the system is proximate to a spin-liquid phase that determines the behavior of excitations except for low energies.[3–5,8] An alternative suggestion is that the continuum might originate from magnon-magnon scattering which is enhanced in noncollinear magnets.[6,7]

In view of the ambiguity in the interpretation of the neutron scattering data, a complementary experimental analysis of the magnetic properties of Cs_2CuCl_4 by a different technique is highly desirable. A very effective and frequently used experimental tool to study low-temperature properties of low-dimensional quantum magnets is the two-magnon Raman scattering.[11–18] The two-magnon Raman intensity is directly related to the spectrum of two interacting magnons in a total spin-zero state at vanishingly small momentum and weighted by a form factor that is dependent on the polarization of the incident light. It contains detailed information on the two-magnon density of states and the magnon-magnon interactions. Therefore, direct comparison of experimental spectra with those obtained from theoretical analysis can lead

to rather accurate estimates on values of the superexchange and DM interactions. In addition, the analysis of the polarization dependence of the magnetic Raman scattering[19,20] might shed some light on whether the ground state is ordered, as neutron scattering experiments have suggested, or is actually in a spin-liquid state, as some theories suggest. A pronounced polarization dependence would indicate that magnetically ordered state is the most probable candidate for the ground state, and that the observed continuum is due to relatively strong interactions between magnons. On the other hand, if the Raman scattering depends weakly on the scattering geometry, the continuum in neutron scattering might be due to unconventional excitations above a spin-liquid ground state.

In this paper, we carry out a theoretical analysis of two-magnon Raman scattering from an anisotropic $S = \frac{1}{2}$ Heisenberg antiferromagnet (HAF) on a triangular lattice (see Fig. 1). To evaluate the two-magnon Raman spectra, we use the well-established, semiphenomenological Loudon-Fleury (LF) approach.[21] By choosing model parameters relevant for the compound Cs_2CuCl_4, we find that the spectral shape as a function of frequency is sensitive to $1/S$ corrections of the magnon spectrum and is strongly modified by the magnon-magnon interactions in the final state. The intensity of the two-magnon peak also significantly depends on the scattering geometry which is in contrast with the polarization independence of the magnetic Raman response in isotropic HAF on the triangular lattice.[19]

The paper is organized as follows. In Sec. II, we present a model of Cs_2CuCl_4 and discuss its classical ground state, which is an incommensurate spin spiral with a pitch vector determined by the competition of anisotropic nearest-neighbor interactions. In Sec. III, we first review results of the one-magnon excitations in the anisotropic $S = \frac{1}{2}$ HAF to first order in $1/S$. We show that although $1/S$ corrections are present in the whole Brillouin zone (BZ), they are less drastic than in the isotropic case of the triangular lattice. This is due to DM interactions, which suppress quantum fluctuations and open a gap at the ordering vector. In Sec. IV, we first review the LF formalism and then use it to calculate the Raman spectra at various levels of approximation, i.e., using only the bare magnon dispersion, using a magnon dispersion renormalized
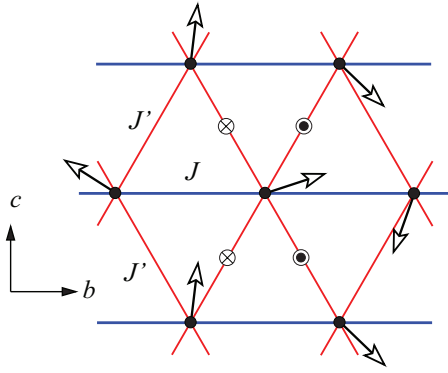
FIG. 1. (Color online) Triangular lattice with anisotropic spin exchanges.

to order $1/S$, and with final-state interactions included. We show that the Raman profile is very sensitive to the magnon-magnon interactions and to the scattering geometry. Finally, Sec. V presents a summary of the work.

II. MODEL

We start with the following spin-$\frac{1}{2}$ model Hamiltonian for Cs_2CuCl_4:

$$H = \sum_{\langle ij \rangle} [J_{ij} \mathbf{S}_i \cdot \mathbf{S}_j + \mathbf{D}_{ij} \cdot (\mathbf{S}_i \times \mathbf{S}_j)], \quad (1)$$

where $\langle ij \rangle$ refers to nearest-neighbor (NN) bonds on the triangular lattice, and J_{ij} and $\mathbf{D}_{ij}$ are the symmetric and antisymmetric exchange constants. The antisymmetric spin exchange originating from the relativistic spin-orbit inter-action is also known as the Dzyaloshinskii-Moriya (DM) interaction. For Cs_2CuCl_4, it is customary to denote the exchange constants J_{ij} along the horizontal bonds, which form quasi-one-dimensional (1D) chains, as J, and J_{ij} along the zigzag bonds as J'.[1,2] In this paper, we consider the DM vectors in the geometry suggested by the neutron-scattering work by Coldea *et al.*[2] In this geometry, the DM interaction vanishes along the quasi-1D chains, whereas on the zigzag bonds, the DM vectors are perpendicular to the triangular plane $\mathbf{D}_{ij} = \pm(0,0,D)$ (Fig. 1). Experimental measurements in high magnetic field have resulted in $J \approx 0.374$ meV, $J' \approx 0.128$ meV, and $D = 0.02$ meV.[2]

The classical ground state of Hamiltonian (1) is given by a spin spiral $\mathbf{S}_i/S = \cos(\mathbf{Q} \cdot \mathbf{r}_i) \hat{\mathbf{b}} + \sin(\mathbf{Q} \cdot \mathbf{r}_i) \hat{\mathbf{c}}$, where the pitch vector $\mathbf{Q} = Q \hat{\mathbf{b}}$ depends on the ratio J'/J. In the isotropic case $J' = J$, the ground state is the well-known $120°$ noncollinear magnetic order with $Q = 2\pi/3$.[22,23] To understand the classical ground state in detail, we consider the energy of the magnetic spiral:

$$E_0(\mathbf{Q}) = 3NS^2 J_{\mathbf{Q}}^T, \quad J_{\mathbf{Q}}^T = J_{\mathbf{Q}} - D_{\mathbf{Q}}, \quad (2)$$

where

$$J_{\mathbf{k}} = \frac{1}{3} \left(J \cos k_y + 2J' \cos \frac{k_y}{2} \cos \frac{\sqrt{3}k_z}{2} \right), \quad (3)$$

$$D_{\mathbf{k}} = \frac{2D}{3} \sin \frac{k_y}{2} \cos \frac{\sqrt{3}k_z}{2}. \quad (4)$$

Minimization with respect to Q leads to the following three types of long-range magnetic order: (1) At $J' > 2J$, the magnetic spiral reduces to collinear Néel order with ferromagnetic ordering of the spins along the chains. Along the c direction, spins on adjacent chains are antiparallel to each other. (2) At $0 < J' \leqslant 2J$, the pitch of the spiral is given by $Q = 2 \arccos(-\frac{J'}{2J})$, which varies from $2\pi \to \pi$ as we vary J' from $2J$ to 0. (3) For $J' = 0$, the system degenerates into decoupled antiferromagnetic chains.

III. LARGE-S EXPANSION

The large-S expansion about the classical spiral order can be significantly simplified with a locally rotated frame of reference.[23] The spin components S_i in a laboratory frame are related to those in the rotated local frame through

$$\begin{aligned} S_i^x &= \tilde{S}_i^x, \\ S_i^y &= \tilde{S}_i^y \cos Q - \tilde{S}_i^z \sin Q, \\ S_i^z &= \tilde{S}_i^y \sin Q + \tilde{S}_i^z \cos Q. \end{aligned} \quad (5)$$

The spiral viewed from the rotated local frame corresponds to a simple ferromagnetic order $\tilde{\mathbf{S}}_i = S\hat{\mathbf{z}}$. We then employ the Holstein-Primakoff transformation

$$\begin{aligned} \tilde{S}_i^z &= S - a_i^+ a_i , \\ \tilde{S}_i^+ &= (2S - a_i^+ a_i)^{1/2} a_i , \\ \tilde{S}_i^- &= a_i^+ (2S - a_i^+ a_i)^{1/2}. \end{aligned} \quad (6)$$

The magnon operators $a_i^\dagger$ and a_i describe excitations around the spiral ground state. As we intend to study magnon interactions to first order in $1/S$, we need to expand the Hamiltonian in Eq. (1) up to quartic order in the boson operators:

$$H = E_0 + 3JS(H_2 + H_3 + H_4). \quad (7)$$

Introducing Fourier transform $a_i = \sum_{\mathbf{k}} a_{\mathbf{k}} e^{i\mathbf{k} \cdot \mathbf{r}_i}/\sqrt{N}$, the explicit expression of the various terms in the Hamiltonian reads as

$$H_2 = \sum_{\mathbf{k}} \left[A_{\mathbf{k}} a_{\mathbf{k}}^\dagger a_{\mathbf{k}} + \frac{B_{\mathbf{k}}}{2} (a_{\mathbf{k}} a_{-\mathbf{k}} + a_{\mathbf{k}}^\dagger a_{-\mathbf{k}}^\dagger) \right], \quad (8)$$

$$H_3 = \frac{i}{2} \sqrt{\frac{1}{2NS}} \sum_{\{\mathbf{k}_i\}} (C_1 + C_2)(a_3^\dagger a_1 a_2 - a_1^\dagger a_2^\dagger a_3), \quad (9)$$

$$\begin{aligned} H_4 = \frac{1}{8NS} \sum_{\{\mathbf{k}_i\}} \Big\{ & [(A_{1-3} + A_{1-4} + A_{2-3} + A_{2-4}) \\ & - (B_{1-3} + B_{1-4} + B_{2-3} + B_{2-4}) \\ & - (A_1 + A_2 + A_3 + A_4)] a_1^\dagger a_2^\dagger a_3 a_4 \\ & - \frac{2}{3}(B_1 + B_2 + B_3)(a_1^\dagger a_2^\dagger a_3^\dagger a_4 + a_4^\dagger a_1 a_2 a_3) \Big\}. \quad (10) \end{aligned}$$

Here, **1** ... **4** denote $\mathbf{k}_1 \ldots \mathbf{k}_4$, and the summation in H_3 and H_4 is subject to momentum conservation $\sum_i \mathbf{k}_i = 0$ up to a reciprocal lattice vector G. The following functions are introduced:

$$\begin{aligned} A_{\mathbf{k}} &= J_{\mathbf{k}} + \frac{1}{2}(J_{\mathbf{Q}+\mathbf{k}}^T + J_{\mathbf{Q}-\mathbf{k}}^T) - 2J_{\mathbf{Q}}^T, \\ B_{\mathbf{k}} &= \frac{1}{2}(J_{\mathbf{Q}+\mathbf{k}}^T + J_{\mathbf{Q}-\mathbf{k}}^T) - J_{\mathbf{k}}, \quad C_{\mathbf{k}} = J_{\mathbf{Q}+\mathbf{k}}^T - J_{\mathbf{Q}-\mathbf{k}}^T. \quad (11) \end{aligned}$$

Here, for convenience, we rescale the interactions $J_{\mathbf{k}}$ and $J_{\mathbf{k}}^T$ with respect to J, which is assumed to be $J = 1$.

The quadratic Hamiltonian H_2 can then be diagonalized by a Bogoliubov transformation:

$$
\begin{aligned}
a_{\mathbf{k}} &= u_{\mathbf{k}} c_{\mathbf{k}} + v_{\mathbf{k}} c_{-\mathbf{k}}^\dagger, \\
a_{\mathbf{k}}^\dagger &= u_{\mathbf{k}} c_{\mathbf{k}}^\dagger + v_{\mathbf{k}} c_{-\mathbf{k}},
\end{aligned} \tag{12}
$$

where $c_{\mathbf{k}}^{(\dagger)}$ are operators for Bogoliubov quasiparticles. The coherence coefficients

$$
u_{\mathbf{k}} = \sqrt{\frac{A_{\mathbf{k}} + E_{\mathbf{k}}}{2E_{\mathbf{k}}}}, \quad v_{\mathbf{k}} = -\frac{B_{\mathbf{k}}}{|B_{\mathbf{k}}|}\sqrt{\frac{A_{\mathbf{k}} - E_{\mathbf{k}}}{2E_{\mathbf{k}}}} \tag{13}
$$

satisfy $u_{\mathbf{k}}^2 - v_{\mathbf{k}}^2 = 1$, and

$$
E_{\mathbf{k}} = \sqrt{A_{\mathbf{k}}^2 - B_{\mathbf{k}}^2} \tag{14}
$$

describes the quasiparticle dispersion (the energy of the quasiparticles is $3JSE_{\mathbf{k}}$). The diagonalized Hamiltonian H_2 is given by

$$
H_2 = E_2(\mathbf{Q}) + \sum_{\mathbf{k}} E_{\mathbf{k}} c_{\mathbf{k}}^\dagger c_{\mathbf{k}}, \tag{15}
$$

where

$$
E_2(\mathbf{Q}) = \sum_{\mathbf{k}} \left(A_{\mathbf{k}} v_{\mathbf{k}}^2 + B_{\mathbf{k}} u_{\mathbf{k}} v_{\mathbf{k}}\right) = -NJ_{\mathbf{Q}}^T + \frac{1}{2}\sum_{\mathbf{k}} E_{\mathbf{k}} \tag{16}
$$

gives the $1/S$ correction to the classical ground-state energy $E_0(\mathbf{Q})$. The $1/S$ correction to the ordering wave vector $\mathbf{Q}$ is determined by minimizing the sum

$$
E_0 + E_2 = 3JS(S-1)NJ_{\mathbf{Q}}^T + \frac{3JS}{2}\sum_{\mathbf{k}} E_{\mathbf{k}} \tag{17}
$$

with respect to Q. The quantum correction is given by

$$
\Delta Q = \frac{-1}{\partial^2 J_Q^T/\partial Q^2}\frac{1}{N}\sum_{\mathbf{k}}\frac{A_{\mathbf{k}} - B_{\mathbf{k}}}{2E_{\mathbf{k}}}\left.\frac{\partial J_{\mathbf{Q}+\mathbf{k}}^T}{\partial Q}\right|_{Q_0}, \tag{18}
$$

where $Q_0 = 2\arccos\left(-\frac{J'}{2J}\right)$ is the pitch of the classical ground state.

The $1/S$ contribution from the quartic Hamiltonian can be obtained through a mean-field decoupling of H_4. We first define

$$
G(\mathbf{k}) = \langle a_{\mathbf{k}}^\dagger a_{\mathbf{k}}\rangle, \quad F(\mathbf{k}) = \langle a_{\mathbf{k}} a_{-\mathbf{k}}\rangle = \langle a_{\mathbf{k}}^\dagger a_{-\mathbf{k}}^\dagger\rangle. \tag{19}
$$

The quadratic Hamiltonian plus the decoupled H_4 can be expressed as

$$
H_2 + \bar{H}_4 = 3JS\sum_{\mathbf{k}}\left[\bar{A}_{\mathbf{k}} a_{\mathbf{k}}^\dagger a_{\mathbf{k}} + \frac{\bar{B}_{\mathbf{k}}}{2}\left(a_{\mathbf{k}} a_{-\mathbf{k}} + a_{\mathbf{k}}^\dagger a_{-\mathbf{k}}^\dagger\right)\right], \tag{20}
$$

where

$$
\begin{aligned}
\bar{A}_{\mathbf{k}} = A_{\mathbf{k}} + \frac{1}{NS}\sum_{\mathbf{q}}\Big[&(A_{\mathbf{k}-\mathbf{q}} + B_{\mathbf{k}-\mathbf{q}} - A_{\mathbf{k}} - A_{\mathbf{q}})G(\mathbf{q}) \\
&- \left(B_{\mathbf{q}} + \frac{B_{\mathbf{k}}}{2}\right)F(\mathbf{q})\Big],
\end{aligned} \tag{21}
$$

$$
\begin{aligned}
\bar{B}_{\mathbf{k}} = B_{\mathbf{k}} + \frac{1}{NS}\sum_{\mathbf{q}}\Big[&-\left(B_{\mathbf{k}} + \frac{B_{\mathbf{q}}}{2}\right)G(\mathbf{q}) \\
&+ \left(A_{\mathbf{k}-\mathbf{q}} + B_{\mathbf{k}-\mathbf{q}} - \frac{A_{\mathbf{q}}}{2} - \frac{A_{\mathbf{k}}}{2}\right)F(\mathbf{q})\Big].
\end{aligned} \tag{22}
$$

The magnon spectrum renormalized by the quartic Hamiltonian H_4 becomes

$$
\bar{E}_{\mathbf{k}} = \sqrt{\bar{A}_{\mathbf{k}}^2 - \bar{B}_{\mathbf{k}}^2} = E_{\mathbf{k}} + \Sigma_{\mathbf{k}}^{(4)} + \mathcal{O}(1/S^2), \tag{23}
$$

where $\Sigma^{(4)}(\mathbf{k})$ is self-energy correction of order $1/S$:

$$
\begin{aligned}
\Sigma_{\mathbf{k}}^{(4)} &= A_{\mathbf{k}}^{(4)}\left(u_{\mathbf{k}}^2 + v_{\mathbf{k}}^2\right) + 2B_{\mathbf{k}}^{(4)} u_{\mathbf{k}} v_{\mathbf{k}} \\
&= \left(A_{\mathbf{k}} A_{\mathbf{k}}^{(4)} - B_{\mathbf{k}} B_{\mathbf{k}}^{(4)}\right)/E_{\mathbf{k}}.
\end{aligned} \tag{24}
$$

To obtain the $1/S$ correction from the cubic Hamiltonian H_3, we follow Ref. 23 and consider interactions between quasiparticles $c, c^\dagger$:

$$
H_3 = \frac{i}{4}\sqrt{\frac{1}{2NS}}\sum_{\{\mathbf{k}_i\}}\left[\Phi_1(\mathbf{k}_1, \mathbf{k}_2; \mathbf{k}_3) c_{\mathbf{k}_1}^\dagger c_{\mathbf{k}_2}^\dagger c_{\mathbf{k}_3} + \frac{1}{3}\Phi_2(\mathbf{k}_1, \mathbf{k}_2, \mathbf{k}_3) c_{\mathbf{k}_1}^\dagger c_{\mathbf{k}_2}^\dagger c_{\mathbf{k}_3}^\dagger\right] + \text{H.c.} \tag{25}
$$

The vertex functions are given by (for simplicity, we denote $1 \equiv \mathbf{k}_1, 2 \equiv \mathbf{k}_2$, etc.)

$$
\Phi_1(1,2;3) = \frac{\tilde{\Phi}_1(1,2;3)}{\sqrt{E_1 E_2 E_3}}, \quad \Phi_2(1,2,3) = \frac{\tilde{\Phi}_2(1,2,3)}{\sqrt{E_1 E_2 E_3}}, \tag{26}
$$

where

$$
\begin{aligned}
\tilde{\Phi}_1(1,2;3) = {}& C_1 f_-^{(1)}\big(f_+^{(2)} f_+^{(3)} + f_-^{(2)} f_-^{(3)}\big) \\
& + C_2 f_-^{(2)}\big(f_+^{(3)} f_+^{(1)} + f_-^{(3)} f_-^{(1)}\big) \\
& + C_3 f_-^{(3)}\big(f_+^{(1)} f_+^{(2)} - f_-^{(1)} f_-^{(2)}\big),
\end{aligned} \tag{27}
$$

$$
\begin{aligned}
\tilde{\Phi}_2(1,2,3) = {}& C_1 f_-^{(1)}\big(f_+^{(2)} f_+^{(3)} - f_-^{(2)} f_-^{(3)}\big) \\
& + C_2 f_-^{(2)}\big(f_+^{(3)} f_+^{(1)} - f_-^{(3)} f_-^{(1)}\big) \\
& + C_3 f_-^{(3)}\big(f_+^{(1)} f_+^{(2)} - f_-^{(1)} f_-^{(2)}\big),
\end{aligned} \tag{28}
$$

and $f_\pm^{(\alpha)} = \sqrt{A_\alpha \pm B_\alpha}$ for $\alpha = 1, 2, 3$.

The triplic contribution to the self-energy is

$$
\begin{aligned}
\Sigma_{\mathbf{k}}^{(3)} = -\frac{1}{16NS}\bigg(&\sum_{\mathbf{k}_1 + \mathbf{k}_2 = \mathbf{k}}\frac{|\Phi^{(1)}(\mathbf{k}_1, \mathbf{k}_2, \mathbf{k})|^2}{E_{\mathbf{k}_1} + E_{\mathbf{k}_2} - E_{\mathbf{k}} + i\eta} \\
&+ \sum_{\mathbf{k}_1 + \mathbf{k}_2 = -\mathbf{k}}\frac{|\Phi^{(2)}(\mathbf{k}_1, \mathbf{k}_2, \mathbf{k})|^2}{E_{\mathbf{k}_1} + E_{\mathbf{k}_2} + E_{\mathbf{k}} + i\eta}\bigg).
\end{aligned} \tag{29}
$$

The first term in Eq. (29) describes a virtual decay of a magnon into two-particle intermediate states. Terms with three creation (annihilation) operators, as will become clear in the next section, play no role in evaluating the magnon interactions within the Raman response. We also note that

$\Sigma_{\mathbf{k}}^{(3)}$ is computed within so-called on-shell approximation. In this approximation, the self-energy is evaluated at the bare magnon energy $E_{\mathbf{k}}$.

Finally, the magnon energy renormalized by both the quartic and the triplic terms is given by

$$\tilde{E}_{\mathbf{k}} = E_{\mathbf{k}} + \Sigma_{\mathbf{k}}^{(4)} + \Sigma_{\mathbf{k}}^{(3)} + \mathcal{O}(1/S^2). \qquad (30)$$

In Fig. 2, we plot the renormalized magnon spectrum $\tilde{E}_{\mathbf{k}}$ for parameters relevant to Cs_2CuCl_4. One can see that the renormalization of the spectrum is much less pronounced than in the case of the isotropic triangular lattice.[24,25] Moreover, the imaginary part of the magnon energy $\text{Im}\tilde{E}_{\mathbf{k}}$ almost vanishes in the whole BZ. Thus, the lifetime of the quasiparticles is very large at almost any momentum. This happens because the DM interaction opens a gap at the ordering $\mathbf{Q}$ vector, which significantly suppresses quantum fluctuations.[7] We note that, as corrections to the ordering vector $\mathbf{Q}$, determined by Eq. (18), are small at those values of D relevant to our calculation, we
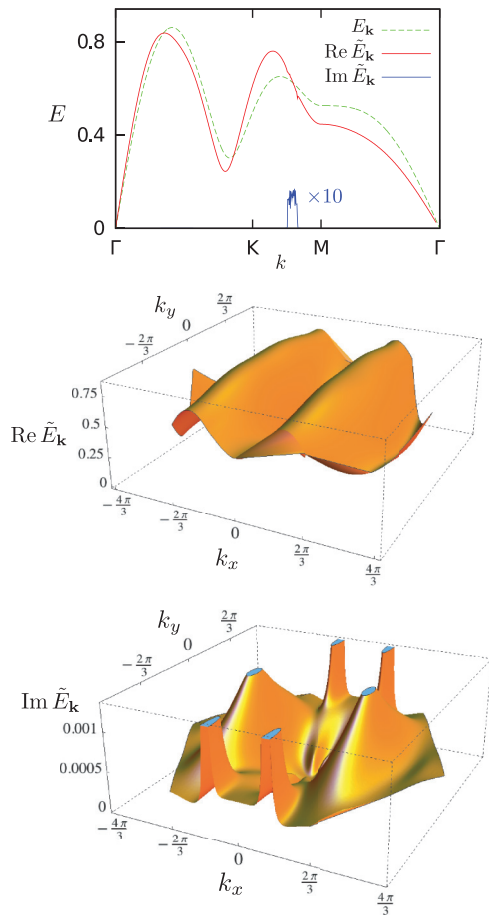

FIG. 2. (Color online) Top: Renormalized magnon dispersion. Dotted line corresponds to the linear spin-wave dispersion $E_{\mathbf{k}}$, while red and blue solid lines correspond to the real and imaginary parts $\text{Re}(\text{Im})\tilde{E}_{\mathbf{k}}$, respectively, computed on a lattice of 252×252 $\mathbf{k}$ points with artificial line broadening of $\eta = 0.003$. Middle and bottom: 3D plot of the $\text{Re}\tilde{E}_{\mathbf{k}}$ and of the $\text{Im}\tilde{E}_{\mathbf{k}}$, respectively. The spectrum is computed for $J = 1$, while other parameters describing interactions Cs_2CuCl_4 are correspondingly rescaled. All energies are measured in units of $3JS$.

use the bare value of the ordering wave vector $\mathbf{Q}_0$ for the remainder of the paper.

IV. RAMAN INTENSITY

A. Loudon-Fleury formalism

Here, we present the analysis of the two-magnon Raman scattering from the anisotropic triangular lattice. We employ the LF approach which models the interaction of light with spin degrees of freedom. The LF scattering operator is given by the photon-induced superexchange operator[21,27]

$$R = \sum_{i,\pm\delta_\mu} (\hat{\boldsymbol{\varepsilon}}_{\text{in}} \cdot \boldsymbol{\delta}_\mu)(\hat{\boldsymbol{\varepsilon}}_{\text{out}} \cdot \boldsymbol{\delta}_\mu) J_\mu \mathbf{S}_i \cdot \mathbf{S}_{i\pm\delta_\mu}, \qquad (31)$$

where $\boldsymbol{\delta}_\mu$ denote basic vectors of triangular lattice: $\boldsymbol{\delta}_1 = (1,0)$, $\boldsymbol{\delta}_2 = (\frac{1}{2}, \frac{\sqrt{3}}{2})$, and $\boldsymbol{\delta}_3 = (-\frac{1}{2}, \frac{\sqrt{3}}{2})$. J_μ defines the Heisenberg exchange on the bond $\boldsymbol{\delta}_\mu$. Since J_μ is anisotropic, the C_{3v} symmetry of the triangular lattice is broken. Thus, instead of using C_{3v}-irreducible representations (A_1, A_2, and E) for characterization of the polarizations, we determine polarizations of incoming and outgoing light as $\hat{\boldsymbol{\varepsilon}}_{\text{in}} = \cos\theta\,\hat{\mathbf{x}} + \sin\theta\,\hat{\mathbf{y}}$ and $\hat{\boldsymbol{\varepsilon}}_{\text{out}} = \cos\phi\,\hat{\mathbf{x}} + \sin\phi\,\hat{\mathbf{y}}$, where θ and ϕ are defined with respect to the x axis.

In terms of Bogoliubov quasiparticle c operators, the LF scattering operator (31) takes the following form:

$$R = \sum_{\mathbf{k}} M_{\mathbf{k}}(c_{\mathbf{k}}c_{-\mathbf{k}} + c_{\mathbf{k}}^\dagger c_{-\mathbf{k}}^\dagger) \equiv r^- + r^+, \qquad (32)$$

where $M_{\mathbf{k}}$ is bare Raman vertex, which is determined by the magnon spectrum and by scattering geometry. The expression for $M_{\mathbf{k}}$ is given by

$$M_{\mathbf{k}} = F_1(\mathbf{k},\theta,\phi)u_{\mathbf{k}}v_{\mathbf{k}} + F_2(\mathbf{k},\theta,\phi)(u_{\mathbf{k}}^2 + v_{\mathbf{k}}^2), \qquad (33)$$

where we introduced the following notations:

$$F_1(\mathbf{k},\theta,\phi) = 2S \sum_{\mu=1}^{3} f_\mu(\theta,\phi)\xi_{\mu\mathbf{k}},$$

$$F_2(\mathbf{k},\theta,\phi) = S \sum_{\mu=1}^{3} f_\mu(\theta,\phi)v_{\mu\mathbf{k}}, \qquad (34)$$

and

$$\xi_{1\mathbf{k}} = \cos k_x(1 + \cos Q_0) - 2\cos Q_0,$$

$$\xi_{2\mathbf{k}} = \cos\left(\frac{k_x}{2} + \frac{\sqrt{3}k_y}{2}\right)\left(1 + \cos\frac{Q_0}{2}\right) - 2\cos\frac{Q_0}{2},$$

$$\xi_{3\mathbf{k}} = \cos\left(\frac{k_x}{2} - \frac{\sqrt{3}k_y}{2}\right)\left(1 + \cos\frac{Q_0}{2}\right) - 2\cos\frac{Q_0}{2},$$

$$v_{1\mathbf{k}} = \cos k_x(1 - \cos Q_0), \qquad (35)$$

$$v_{2\mathbf{k}} = \cos\left(\frac{k_x}{2} + \frac{\sqrt{3}k_y}{2}\right)\left(1 - \cos\frac{Q_0}{2}\right),$$

$$v_{3\mathbf{k}} = \cos\left(\frac{k_x}{2} - \frac{\sqrt{3}k_y}{2}\right)\left(1 - \cos\frac{Q_0}{2}\right).$$

The functions $f_\mu(\theta,\phi) \equiv (\hat{\boldsymbol{\varepsilon}}_{\text{in}} \cdot \boldsymbol{\delta}_\mu)(\hat{\boldsymbol{\varepsilon}}_{\text{out}} \cdot \boldsymbol{\delta}_\mu)$ are symmetry weighting factors along the three basic vectors $\boldsymbol{\delta}_\mu$ of the triangular lattice.

The Raman intensity is obtained from the Fermi's golden rule, which on the imaginary frequency axis reads as

$$I(\omega_m) \simeq \mathrm{Im}\left[\int_0^\beta d\tau\, e^{i\omega_m\tau}\,\langle T_\tau(R(\tau)R)\rangle\right]. \quad (36)$$

By analytically continuing Matsubara frequencies $\omega_m = 2\pi mT$ onto the real axis as $i\omega_m \to \Omega + i\eta$, we obtain the Raman intensity as a function of the inelastic energy transfer $\Omega = \omega_{\mathrm{in}} - \omega_{\mathrm{out}}$ of the incident photons. For the rest of the paper, we assume the temperature $T = 1/\beta$ to be zero.

To order $1/S$, the Raman polarization operator $\langle T_\tau(R(\tau)R)\rangle$ contains only terms such as $\langle T_\tau(r^+(\tau)r^-)\rangle + \langle T_\tau(r^-(\tau)r^+)\rangle$, where $r^\pm$ are specified in Eq. (32) and Fig. 5(a). By Hermitian conjugation, it is sufficient to calculate $J(\tau) = \langle T_\tau(r^-(\tau)r^+)\rangle$, which is depicted in Fig. 5(b).

B. Raman intensity without final-state interactions

We now focus on the contribution from two-magnon Raman scattering, which can be computed at different levels of approximation. We begin by first using only the bare spin-wave dispersion. Then, we continue by including renormalizations of the one-magnon spectrum to $1/S$ order. Calculating the Raman polarization operator $\langle T_\tau(R(\tau)R)\rangle$ with the bare propagators of the Bogoliubov quasiparticles $G(\mathbf{k}, i\omega_n) = 1/(i\omega_n - E_\mathbf{k})$, where $E_\mathbf{k}$ is the bare magnon spectrum, gives the following expression for the Raman intensity:

$$
\begin{aligned}
&I(\Omega) \\
&\simeq \mathrm{Im}\left[\int d^2\mathbf{k} \int \frac{d\omega}{2\pi} M_\mathbf{k}^2 \frac{1}{\iota\omega - E_\mathbf{k}} \frac{1}{\iota(\Omega - \omega) - E_\mathbf{k}}\right]\Bigg|_{\Omega \to -i\Omega + \eta} \\
&= -\mathrm{Im}\left[\int d^2\mathbf{k}\, M_\mathbf{k}^2 \frac{1}{\Omega - 2E_\mathbf{k} + \iota\eta}\right] \\
&= \eta \int d^2\mathbf{k}\, M_\mathbf{k}^2 \frac{1}{(\Omega - 2E_\mathbf{k})^2 + \eta^2}. \quad (37)
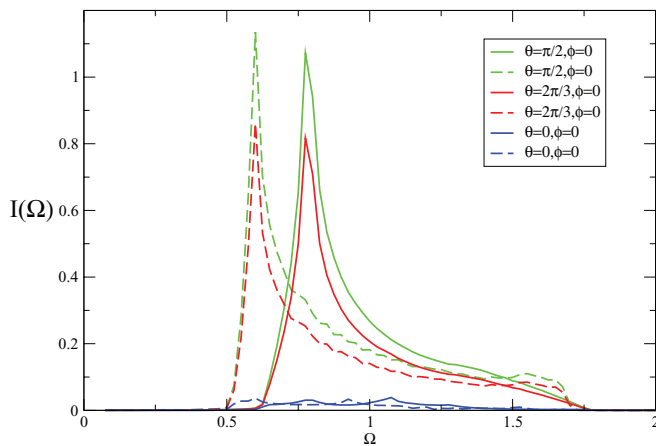\end{aligned}
$$

FIG. 3. (Color online) Bare Raman intensity (solid lines) and Raman intensity including the one-magnon renormalization of the spectrum (dashed lines) at different polarizations of light described by ϕ, and θ scattering angles. Number of $\mathbf{k}$ points: 252×252. The broadening parameter is $\eta = 0.003$. Ω is measured in units of $3JS$.

Figure 3 shows the bare Raman spectra (solid lines) as functions of the transferred photon frequencies Ω for three scattering geometries: (i) $\theta = \pi/2, \phi = 0$, (ii) $\theta = 2\pi/3, \phi = 0$, and (iii) $\theta = 0, \phi = 0$. For two of the polarizations (i) and (ii), the Raman spectra show a similar profile and intensity: the Raman response exhibits a peak at $\Omega \simeq 0.8$–0.9, and the location of this peak corresponds to twice the energy of the dominant van Hove singularity of the one-magnon dispersion (cf. Fig. 2).

The small Raman intensity $I(\Omega)$ at low energies is due to two reasons. First, the magnon energy is gapless only at the zone center and has a gap caused by the DM interaction at the ordering wave vector $\mathbf{Q}_0$. Thus, only magnons with momentum near $\mathbf{k} \simeq 0$ can be excited by photons with frequency $\Omega < 2E(\mathbf{Q}_0)$. As one can see from Fig. 2, the rather steep magnon spectrum in the vicinity of zone center gives rise to a small density of states. Second, the form of $M_\mathbf{k}^2$ is such that it selects mostly wave vectors $k \sim \pi$ where the gap resides.

In the $\theta = \phi = 0$ geometry, the Raman response is nonvanishing but very small for the whole energy range compared with intensities observed in other geometries. The relative smallness can be understood by comparing this result with the well-studied case of the square lattice, for which the LF operator in the A_{1g} geometry commutes with the Heisenberg Hamiltonian, and, as a result, the Raman response vanishes. In the case of the anisotropic triangular lattice, a noncommuting part of the LF operator (31) remains nonzero even for the A_{1g} geometry. This part leads to small Raman intensities, scaling with the ratio $(J'/J)^2$. Indeed, as we have discussed earlier, the anisotropic triangular lattice can be viewed as an interpolation between the square and the isotropic triangular lattice by varying J'/J.

In Fig. 4, the two-magnon peak is shown as a function of the scattering angle θ. A strong dependence on the scattering geometry can be seen: the largest peak intensity is observed at the $\theta = \pi/2, \phi = 0$, i.e. cross polarization, which gradually decreases and reaches its minimum at $\theta = 0$ or π (although not exactly, the peak intensity is roughly proportional to $\sin^2\theta$). This polarization dependence is consistent with the fact that the anisotropy in the present case resembles more that of a rectangular than of an isotropic triangular geometry.
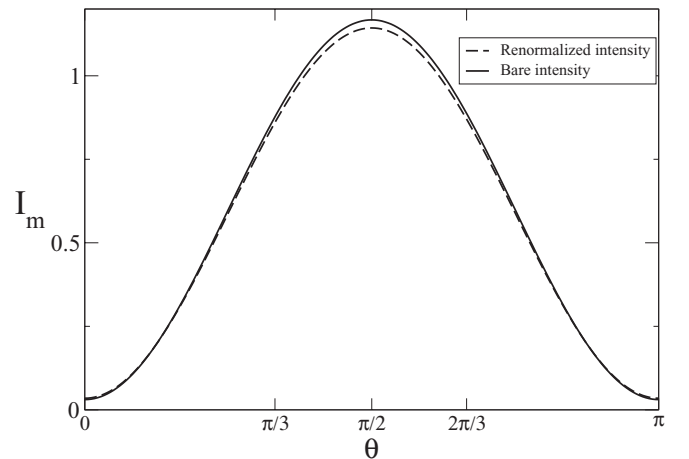

FIG. 4. Variation of the maximum of the bare and renormalized intensities as a function of the scattering angle θ computed at $\Omega = 0.8$ and 0.6, respectively.

An angular-dependence analysis of the Raman spectrum on Cs$_2$CuCl$_4$ is highly desirable as it could provide a potential diagnosis of whether a long-range spin order develops in the ground state. If an angular dependence similar to the one described above is observed, then the ground state is likely to be an incommensurate spiral.[6,7] On the other hand, a Raman response that is independent of the scattering geometry might indicate a spin-liquid ground state,[20] as proposed in some recent theories.[3–5,8] Here, some precautions are necessary. Since the underlying Hamiltonian is spatially anisotropic, the spinon excitations of the proposed spin-liquid phase might inherit the crystal anisotropy to some degree, hence also giving rise to a polarization-dependent Raman signal. This question should be further studied but we believe that even if this is the case, the polarization dependence of the Raman response will be much weaker than in the case of spiral magnetic order.

Next, we incorporate $1/S$ corrections to the Raman spectrum. This can be easily done by replacing the bare energy with the renormalized magnon energy $\tilde{E}_\mathbf{k}$ (30) in the propagator $G(\mathbf{k},i\omega_n) = 1/(i\omega_n - \tilde{E}_\mathbf{k})$. The renormalized Raman spectra are shown by dashed lines in Fig. 3. We can see that in the renormalized spectrum the two-magnon peak appears at the energy $\Omega \simeq 0.6$, which is slightly lower than the peak in the bare spectrum. This is in contrast with the case of isotropic triangular lattice, where the peak is shifted to higher energies. Once again, it shows that the Raman spectra on the anisotropic triangular lattice has features of both triangular and square lattices.

C. Raman intensity with final-state interactions

Next, we consider the final-state magnon-magnon interactions. Usually, these are not small, particularly for $S = \frac{1}{2}$. The effect of the final-state magnon-magnon interactions can be taken into account by computing vertex corrections to the bare Raman vertex. Here, we consider only the leading $1/S$ corrections. In this approximation, the vertex corrections can be obtained from an infinite summation of ladder diagrams. These ladder diagrams are shown in Fig. 5(c) in terms of the two-particle (ir)reducible Raman vertex $[\gamma(\mathbf{k},\mathbf{p},\omega_n,\omega_o)]\Gamma(\mathbf{k},\omega_n,\omega_m)$. These are related by the Bethe-Salpeter equation

$$\Gamma(\mathbf{k},\omega_n,\omega_m) = r^-(\mathbf{k}) + \sum_{\mathbf{p},\omega_o} \gamma(\mathbf{k},\mathbf{p},\omega_n,\omega_o)$$
$$\times G(\mathbf{p},\omega_o + \omega_m)G(-\mathbf{p}, -\omega_o)\Gamma(\mathbf{p},\omega_o,\omega_m).$$
$$(38)$$

The two-particle irreducible vertex can be decomposed as in Fig. 5(d): $\gamma(\mathbf{k},\mathbf{p},\omega_n,\omega_o) = \gamma_3(\mathbf{k},\mathbf{p},\omega_n,\omega_o) + \gamma_4(\mathbf{k},\mathbf{p})$. The quartic vertex $\gamma_4(\mathbf{k},\mathbf{p})$ is identical to the two-particle–two-hole contribution from the H_4 term; its explicit expression is given by

$$\gamma_4(\mathbf{k},\mathbf{p}) = \frac{1}{4S}\big[4(A_0 - B_0 + A_{\mathbf{p}+\mathbf{k}} - B_{\mathbf{p}+\mathbf{k}}$$
$$+ A_\mathbf{p} - A_\mathbf{k})u_\mathbf{p}u_\mathbf{k}v_\mathbf{p}v_\mathbf{k} + (A_{\mathbf{p}-\mathbf{k}} - B_{\mathbf{p}-\mathbf{k}}$$
$$+ A_{\mathbf{p}+\mathbf{k}} - B_{\mathbf{p}+\mathbf{k}} - A_\mathbf{p} - A_\mathbf{k})(u_\mathbf{p}^2 u_\mathbf{k}^2 + v_\mathbf{p}^2 v_\mathbf{k}^2)$$
$$- (2B_\mathbf{p} + B_\mathbf{k})(u_\mathbf{p}^2 + v_\mathbf{p}^2)u_\mathbf{k}v_\mathbf{k}$$
$$- (2B_\mathbf{k} + B_\mathbf{p})(u_\mathbf{k}^2 + v_\mathbf{k}^2)u_\mathbf{p}v_\mathbf{p}\big],$$
$$(39)$$

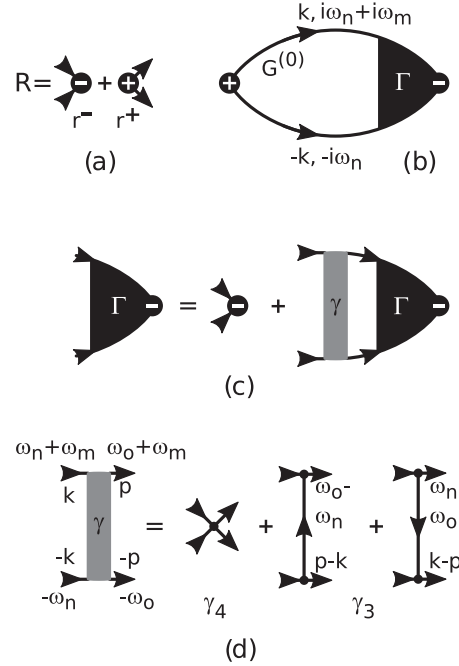where the functions $A_\mathbf{k}$ and $B_\mathbf{k}$ are given by Eqs. (11).

FIG. 5. (a) Bare Raman vertex R from Eq. (32); (b) Raman susceptibility bubble; (c) the integral equation for the dressed Raman vertex Γ in terms of the irreducible magnon particle-particle vertex γ; (d) leading-order $1/S$ contributions to γ.

The triplic vertex $\gamma_3(\mathbf{k},\mathbf{p},\omega_n,\omega_o)$ is obtained from the product of two vertices of the cubic term H_3 and one intermediate propagator, and can be written as

$$\gamma_3(\mathbf{k},\mathbf{p},\omega_n,\omega_o) = \frac{1}{32S}\,[\Phi_1(\mathbf{p},\mathbf{k}-\mathbf{p};\mathbf{k})\Phi_1^*(\mathbf{p},\mathbf{k}-\mathbf{p};\mathbf{k})$$
$$\times G^0(\mathbf{k}-\mathbf{p},i\omega_o - i\omega_n)$$
$$+ \Phi_1(-\mathbf{p},\mathbf{p}-\mathbf{k};-\mathbf{k})\Phi_1^*(-\mathbf{p},\mathbf{p}-\mathbf{k};-\mathbf{k})$$
$$\times G^0(\mathbf{p}-\mathbf{k},i\omega_n - i\omega_o)],$$
$$(40)$$

where the functions $\Phi_1(1,2;3)$ and their complex conjugates are given by Eqs. (26) and (27). To keep $\gamma_3(\mathbf{k},\mathbf{p},\omega_n,\omega_o)$ to leading order in $1/S$, we retained only the zeroth-order propagators G^0 for each intermediate line. We further simplify the expression (40) by assuming that the dominant contribution to the frequency summations in the Bethe-Salpeter equation (38) comes from the mass shell of the intermediate particle-particle propagators. This corresponds to the substitution of the intermediate frequencies by $-i\omega_n \approx E_\mathbf{k}, -i\omega_o \approx E_\mathbf{p}$. The simplified expression for the triplic vertex then reads as

$$\gamma_3(\mathbf{k},\mathbf{p}) \simeq \frac{1}{32S}\,\Phi_1(\mathbf{p},\mathbf{k}-\mathbf{p};\mathbf{k})\,\Phi_1^*(-\mathbf{p},\mathbf{p}-\mathbf{k};-\mathbf{k})$$
$$\times \frac{2E_{\mathbf{k}-\mathbf{p}}}{(E_\mathbf{k} - E_\mathbf{p})^2 - E_{\mathbf{k}-\mathbf{p}}^2}.$$
$$(41)$$

The triplic vertex then depends only on momenta.

Next, we perform the frequency summation over ω_o on the right-hand side of Eq. (38) as well as the analytic continuation $i\omega_m \to \Omega + i\eta \equiv z$. With this, the reducible vertex Γ in the latter equation turns into a function of $\mathbf{p}$ and z only,

leading to

$$\sum_{\mathbf{p}} L_{\mathbf{k},\mathbf{p}}(z)\Gamma_{\mathbf{p}}(z) = r^-(\mathbf{k}), \tag{42}$$

$$L_{\mathbf{k},\mathbf{p}}(z) = \delta_{\mathbf{k},\mathbf{p}} - \frac{\gamma(\mathbf{k},\mathbf{p})}{z - 2\tilde{E}_{\mathbf{p}}}, \tag{43}$$

which is an integral equation with respect to momentum only. Finally, the expression for the Raman intensity can be written as

$$I(\Omega) \simeq [J(\Omega) - J(-\Omega)], \tag{44}$$

where

$$J(\Omega) = \text{Im}\left[\sum_{\mathbf{k}} \frac{M_{\mathbf{k}}\,\Gamma_{\mathbf{k}}(\Omega + i\eta)}{\Omega + i\eta - 2\tilde{E}_{\mathbf{k}}}\right]. \tag{45}$$

The fully renormalized intensity for the polarization with $\theta = 2\pi/3, \phi = 0$ is shown in Fig. 6(a). Despite the damping by the vertex corrections, the two-magnon peak survives and is further shifted towards lower energies. Apparently, the damping of the peak is less pronounced compared with the isotropic triangular lattice case.[19] At the higher energies, we also see the appearance of a broad continuum. We would like to point out that both the peak and the broad continuum are observed in geometries with almost perpendicular $\hat{\boldsymbol{\varepsilon}}_{\text{in}}$ and $\hat{\boldsymbol{\varepsilon}}_{\text{out}}$. Although the width and intensities of the peak and the profile of the continuum vary with the angle θ, the position of the two-magnon peak and the center of the continuum do not change significantly for $\theta \sim \pi/2$. On the other hand, the Raman signal is extremely weak for nearly parallel geometries ($\theta, \phi \sim 0$), similar to the case without vertex corrections (see Fig. 3).

In order to disentangle the contributions coming from the triplic and quartic terms, we also compute the Raman spectrum with an irreducible vertex which includes only the quartic part. The comparison between the Raman spectrum computed with the full vertex and with the one containing only $\gamma_4(\mathbf{k},\mathbf{p})$ is presented in Fig. 6(b). One observes that vertex corrections due to the quartic term split the sharp two-magnon peak into two peaks of comparable intensities, which are, however, about the half of the intensity of the two-magnon peak with final-state interactions. The triplic term modifies these two peaks quite differently. The lower-energy peak is only weakly renormalized by the triplic term, while the higher-energy peak is damped more strongly and is transformed into the broad continuum.

Finally, we note that the direct comparison of these results with Fig. 3 should be taken with a certain precaution since the artificial line broadening in Fig. 6 is larger by one order of magnitude. This is a consequence of a factor of 16 less $\mathbf{k}$ points used in the latter case. This is because the kernel $L_{\mathbf{k},\mathbf{p}}(z)$ in the integral equations (42) and (43) is not sparse and has rank $N^2 \times N^2$. Consequently, a moderate lattice size gives rise to a rather large dimension for the kernel. In the above calculations, we have chosen $N = 69$, leading to a 4761×4761 system which we have solved 100 times to account for 100 frequencies in the interval $\Omega \in [0,2]$. We also note that the kernel has points of singular behavior in $(\mathbf{k},\mathbf{p})$-space, which stem from the singularities of the Bogoliubov factors and from the energy denominators in vertex functions. Here, we have chosen to
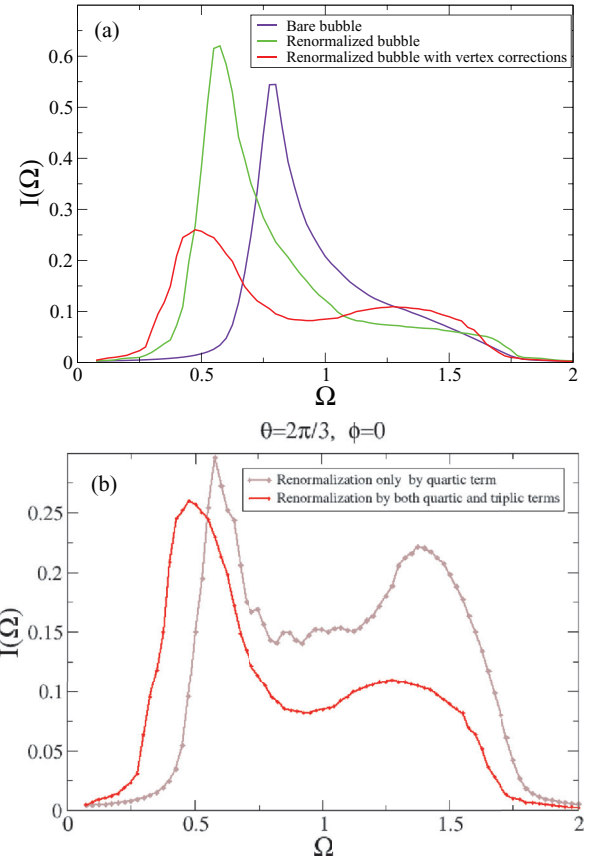

FIG. 6. (Color online) Effect of final-state interactions on Raman intensity for $\theta = 2\pi/3, \phi = 0$. (a) Bare intensity, an intensity computed with renormalized magnon energies, and intensity computed with included final-state interactions are shown by blue, green, and red lines, respectively. Number of $\mathbf{k}$ points: 69×69. The imaginary broadening is $\eta = 0.03$. Ω is measured in units of $3JS$. (b) Comparison of the intensities computed with corrections only due to the quartic vertex $\gamma_4(\mathbf{k})$ (brown solid line with diamonds), and with corrections due to full vertex $\gamma_3(\mathbf{k}) + \gamma_4(\mathbf{k})$ (red solid line with circles).

regularize these points by cutting off eventual singularities in $L_{\mathbf{k},\mathbf{p}}$. This can be justified because the weight of these points is negligibly small compared with the total number of points in the BZ. We have checked that this regularization does not significantly effect the obtained spectra.

V. SUMMARY

In summary, we have studied the two-magnon Raman scattering in the anisotropic triangular Heisenberg antiferromagnet considering various levels of approximation within a controlled $1/S$ expansion. We have shown that the Raman profile is sensitive to the magnon-magnon interactions and to the scattering geometry. The calculations indicate that the main effect of the magnon-magnon interactions is on the shifting of the two-magnon peak towards lower energies and on the formation of the broad continuum at the higher energies. We have also shown that through exchange and DM interactions, the spatial anisotropy of the lattice is transferred to the magnon dispersion of the spiral magnetic order. This makes the

two-magnon Raman scattering anisotropic and very sensitive to the scattering geometry when the spiral magnetic order is the ground state. Our results on the polarization dependence of the spectrum suggest that Raman spectroscopy might be very useful to resolve the ambiguity in the interpretation of the neutron scattering experiments and to gain insight into the magnetic structure of Cs_2CuCl_4.

As a final note, in this paper we have used as an input the orientation of the DM vectors extracted from neutron scattering in Ref. 2. Recent electron spin resonance (ESR) measurements by Povarov *et al.*[17] suggested an alternative orientation of the DM vectors in Cs_2CuCl_4, in which the strongest DM interaction is along the spin chains. It is worth noting that the two different sets of the DM vectors give rise to the same spin order in the classical ground state of the Heisenberg model on the anisotropic triangular lattice. The direction of the DM vectors is particularly important for magnetic properties of Cs_2CuCl_4 in the presence of the magnetic field because both the magnetic ground state and the excitation spectra in this case depend on the relative orientation of the external field and the direction of the DM vector.[9,17,18] While the zero-field magnon spectrum certainly depends on the orientations of the DM vectors, the main conclusion of this paper remains valid, namely, a polarization-dependent Raman signal in the magnetically ordered ground state. Moreover, since the main effect of DM interactions is the opening of the spectral gap at the ordering wave vector, the higher-energy magnon excitations that contribute most to the Raman signal are not strongly affected by different geometries of the DM vectors.

[1] R. Coldea, D. A. Tennant, K. Habicht, P. Smeibidl, C. Wolters, and Z. Tylczynski, Phys. Rev. Lett **88**, 137203 (2002).

[2] R. Coldea, D. A. Tennant, and Z. Tylczynski, Phys. Rev. B **68**, 134424 (2003).

[3] S. V. Isakov, T. Senthil, and Yong Baek Kim, Phys. Rev. B **72**, 174417 (2005).

[4] Jason Alicea, Olexei I. Motrunich, and Matthew P. A. Fisher, Phys. Rev. Lett. **95**, 247203 (2005); Phys. Rev. B **73**, 174430 (2006).

[5] S. Yunoki and S. Sorella, Phys. Rev. B **74**, 014408 (2006).

[6] M. Y. Veillette, A. J. A. James, and F. H. L. Essler, Phys. Rev. B **72**, 134429 (2005).

[7] D. Dalidovich, R. Sknepnek, A. J. Berlinsky, J. Zhang, and C. Kallin, Phys. Rev. B **73**, 184403 (2006).

[8] O. A. Starykh and L. Balents, Phys. Rev. Lett **98**, 077205 (2007).

[9] Oleg A. Starykh, Hosho Katsura, and Leon Balents, Phys. Rev. B **82**, 014421 (2010).

[10] Andreas Kreisel, Peter Kopietz, Pham Thanh Cong, Bernd Wolf, and Michael Lang, Phys. Rev. B **84**, 024414 (2011).

[11] A. Gozar, B. S. Dennis, H. Kageyama, and G. Blumberg, Phys. Rev. B **72**, 064405 (2005).

[12] F. Vernay, T. P. Devereaux, and M. J. P. Gingras, J. Phys.: Condens. Matter **19**, 145243 (2007).

[13] Kwang-Yong Choi, Hiroyuki Nojiri, Naresh S. Dalal, Helmuth Berger, Wolfram Brenig, and Peter Lemmens, Phys. Rev. B **79**, 024416 (2009).

[14] M. N. Iliev, A. P. Litvinchuk, V. G. Hadjiev, M. M. Gospodinov, V. Skumryev, and E. Ressouche, Phys. Rev. B **81**, 024302 (2010).

[15] X. Wang, K. Syassen, M. Johnsson, R. Moessner, K.-Y. Choi, and P. Lemmens, Phys. Rev. B **83**, 134403 (2011).

[16] C.-C. Chen, C. J. Jia, A. F. Kemper, R. R. P. Singh, and T. P. Devereaux, Phys. Rev. Lett. **106**, 067002 (2011).

[17] K. Yu. Povarov, A. I. Smirnov, O. A. Starykh, S. V. Petrov, and A. Ya. Shapiro, Phys. Rev. Lett. **107**, 037204 (2011).

[18] A. I. Smirnov, K. Yu. Povarov, S. V. Petrov, and A. Ya. Shapiro, Phys. Rev. B **85**, 184423 (2012).

[19] N. Perkins and W. Brenig, Phys. Rev. B **77**, 174412 (2008).

[20] O. Cépas, J. O. Haerter, and C. Lhuillier, Phys. Rev. B **77**, 172406 (2008).

[21] A. Fleury and R. Loudon, Phys. Rev. **166**, 514 (1968).

[22] Th. Jolicoeur and J. C. Le Guillou, Phys. Rev. B **40**, 2727 (1989).

[23] A. V. Chubukov, S. Sachdev, and T. Senthil, J. Phys.: Condens. Matter **6**, 8891 (1994).

[24] Oleg A. Starykh, Andrey V. Chubukov, and Alexander G. Abanov, Phys. Rev. B **74**, 180403(R) (2006).

[25] A. L. Chernyshev and M. E. Zhitomirsky, Phys. Rev. Lett. **97**, 207202 (2006).

[26] L. Benfatto, M. B. Silva Neto, A. Gozar, B. S. Dennis, G. Blumberg, L. L. Miller, Seiki Komiya, and Yoichi Ando, Phys. Rev. B **74**, 024416 (2006).

[27] Here, we note that in the presence of the spin-orbit coupling giving rise to the DM interaction, the effective Hamiltonian (31) describing the interaction of light with magnons shall also contain an antisymmetric part (Refs. 21 and 26). This term contributes only to the one-magnon Raman response which we do not describe here. This is the reason why we did not include the antisymmetric term in Eq. (31).